

Revealing the Size-Dependent d–d Excitations of Cobalt Nanoparticles Using Soft X-ray Spectroscopy

Zhangzhang Cui,^{†,‡} Chenlu Xie,[§] Xuefei Feng,^{||} Nigel Becknell,[§] Peidong Yang,^{§,⊥} Yalin Lu,^{†,‡,#} Xiaofang Zhai,^{†,‡} Xiaosong Liu,^{||} Wanli Yang,[▽] Yi-De Chuang,^{*,▽} and Jinghua Guo^{*,▽,○}

[†]Hefei National Laboratory for Physical Sciences at the Microscale and Department of Materials Science and Engineering, University of Science and Technology of China, Hefei 230026, Anhui, China

[‡]Synergetic Innovation Center of Quantum Information and Quantum Physics, University of Science and Technology of China, Hefei 230026, Anhui, China

[§]Department of Chemistry, University of California, Berkeley, California 94720, United States

^{||}State Key Laboratory of Functional Materials for Informatics, Shanghai Institute of Microsystem and Information Technology, Chinese Academy of Science, Shanghai 200050, China

[⊥]Materials Sciences Division, Lawrence Berkeley National Laboratory, Berkeley, California 94720, United States

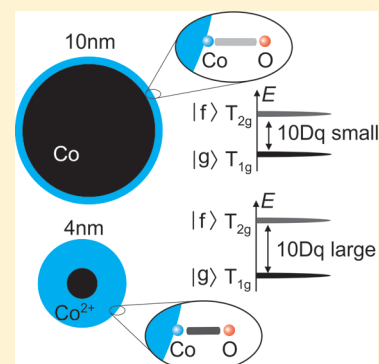
[#]National Synchrotron Radiation Laboratory, University of Science and Technology of China, Hefei 230026, Anhui, China

[▽]Advanced Light Source, Lawrence Berkeley National Laboratory, Berkeley, California 94720, United States

[○]Department of Chemistry and Biochemistry, University of California, Santa Cruz, California 95064, United States

S Supporting Information

ABSTRACT: Cobalt-based catalysts are widely used to produce liquid fuels through the Fischer–Tropsch (FT) reaction. However, the cobalt nanocatalysts can exhibit intriguing size-dependent activity whose origin remains heavily debated. To shed light on this issue, the electronic structures of cobalt nanoparticles with size ranging from 4 to 10 nm are studied using soft X-ray absorption (XAS) and resonant inelastic X-ray scattering (RIXS) spectroscopies. The RIXS measurements reveal the significant size-dependent d–d excitations, from which we determine that the crystal-field splitting energy $10Dq$ changes from 0.6 to 0.9 eV when the particle size is reduced from 10 to 4 nm. The finding that larger Co nanoparticles have smaller $10Dq$ value is further confirmed by the Co L-edge RIXS simulations with atomic multiplet code. Our RIXS results demonstrate a stronger Co–O bond in smaller Co nanoparticles, which brings in further insight into their size-dependent catalytic performance.



Cobalt-based catalysts are well known for their prominent activity and selectivity in the Fischer–Tropsch (FT) synthesis, and their physical and chemical properties have been studied extensively over the past decades.^{1,2} One crucial factor that influences their catalytic performance in the FT reaction, in particular for Co metal nanocatalysts, is the particle size. It is demonstrated that the reactivity and selectivity of Co nanoparticles toward long-chain hydrocarbon is optimum at the size of ~ 10 nm, but that decreases rapidly when the particle size is below 6–8 nm.^{3,4} The origin of this size effect is still heavily debated, despite the tremendous research efforts that have been devoted to this subject thus far. Some studies attributed this size effect to the low reducibility and high reoxidation tendency of smaller Co nanoparticles, as the metallic Co^0 are the active sites in the FT reaction.^{5,6} Other studies demonstrated that the dissociation of carbon monoxide (CO) and hydrogen (H_2) is dependent on the size of Co nanoparticles, which leads to variation in the catalytic activity and selectivity.^{4,7–9} Additionally, the size-dependent metal

surface reconstruction under FT condition was believed to be another relevant factor.^{3,10,11}

An essential prerequisite for gaining further insight into this size effect is the probing of fine electronic structures of Co nanoparticles as a function of particle size. The electronic structures of active Co 3d electrons can be strongly influenced by the local environment around Co atom. For example, the Co 3d electrons in CoO with octahedral symmetry (O_h) will have ${}^4T_{1g}({}^4F)$, ${}^4T_{2g}({}^4F)$, and ${}^4A_{2g}({}^4F)$ multiplet states (Figure 1a), and the energies of these multiplet states set by the geometric configurations and local chemical environment affect the physical and chemical properties of the compound. Although such information may be obtained from fitting the soft X-ray absorption spectra (XAS) of Co nanoparticles, the core-hole lifetime involved in the XAS process broadens the spectral line

Received: November 7, 2016

Accepted: December 21, 2016

Published: December 21, 2016

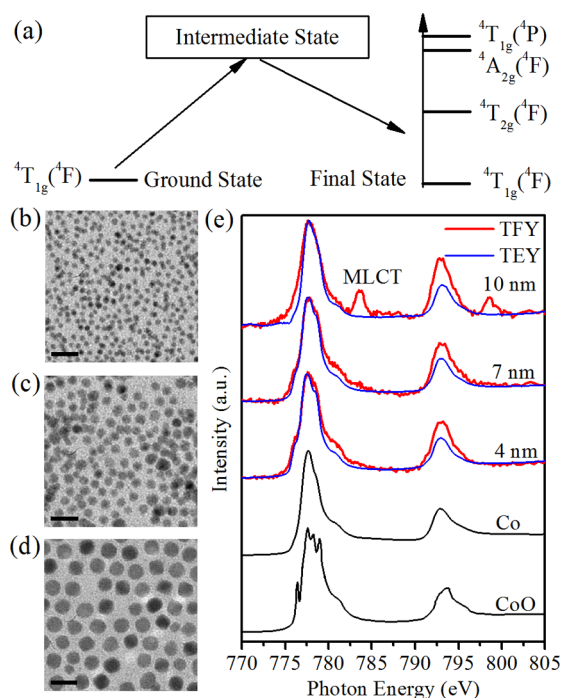


Figure 1. (a) Schematic illustration of RIXS process in CoO with O_h symmetry, where transition takes place from ground state ${}^4T_{1g}({}^4F)$ to intermediate and to ${}^4T_{1g}({}^4F)$ (elastic line), ${}^4T_{2g}({}^4F)$, ${}^4A_{2g}({}^4F)$, and ${}^4T_{1g}({}^4P)$ final states. TEM images of (b) 4, (c) 7, and (d) 10 nm Co nanoparticles. The horizontal bar in these images denotes the 20 nm length scale. (e) Normalized XAS spectra of 4, 7, and 10 nm Co nanoparticles recorded in TEY (thin blue curves) and TFY (thick red curves) modes, together with the reference spectra of CoO and Co metal samples (black curves).

shape, limiting the precise determination of multiplet state energies.

Resonant inelastic X-ray scattering (RIXS) spectroscopy has been extensively used to probe the d–d transitions between these multiplet states in the correlated materials. RIXS is a second-order optical process that involves the excitation of

electrons from core levels to the unoccupied states (photon absorption) followed by the de-excitation of other electrons in the occupied states back to the core levels (photon emission).^{12–14} Unlike XAS, the energy resolution of RIXS, because of the superposition of photon absorption and emission processes, is not limited by the core-hole lifetime.¹⁵ Depending on the symmetry of ground, intermediate, and final states (see Figure 1a), the intensity and energy (or energy loss relative to the elastic line) of RIXS features enable the direct measurement of multiplet states of 3d electrons of Co nanoparticles.

In this study, we performed the systematic investigations of electronic structures of Co nanoparticles as a function of particle size using XAS and RIXS at both Co M- and L-edges. Our XAS and RIXS results show that the surface Co atoms in larger nanoparticles are more resistant to oxidation. Furthermore, the RIXS measurements clearly reveal the significant size-dependent d–d excitations, from which we determine that the crystal-field splitting energy $10Dq$ is reduced in larger Co nanoparticles. These results are further confirmed by simulating the L-edge RIXS spectra with atomic multiplet code. Our results suggest the strong modulation of electronic structures by the Co nanoparticle size, which can provide novel insight into their size-dependent catalytic performance.

The transmission electron microscopy (TEM) images of 4, 7, and 10 nm Co nanoparticles are shown in Figure 1b–d. All TEM images display narrow size distributions, and the exact nanoparticle sizes are determined to be 4.01 ± 0.67 , 6.57 ± 0.67 , and 9.81 ± 0.79 nm, respectively. The histograms for the size distribution of these nanoparticles are shown in Figure S1 in the Supporting Information. The TEM results confirm the precise nanoparticle size-control by the heating temperature in the synthesis process (see Methods section). The Co L-edge XAS of these nanoparticles recorded in total electron yield (TEY, thin blue curves) and total fluorescence yield (TFY, thick red curves) modes are shown in Figure 1e, together with the reference spectra of CoO and Co metal samples (black curves). The XAS spectra in TFY mode exhibit higher $L_2/(L_2 + L_3)$ branching ratio than that of TEY mode, which is due to the saturation effect in the fluorescence detection method.¹⁶ Two

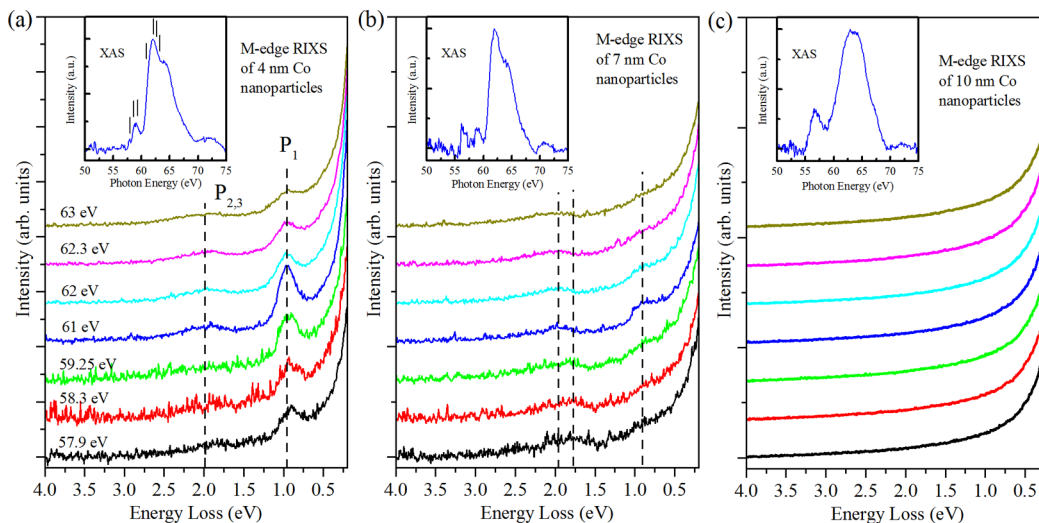


Figure 2. M-edge RIXS spectra of (a) 4, (b) 7, and (c) 10 nm Co nanoparticles. The insets show the corresponding M-edge XAS spectra. The incident photon energies for the RIXS spectra are listed in panel a and are also indicated by vertical ticks in the inset of panel a. Traces with same color have the same incident photon energies. Peaks P_1 , P_2 , and P_3 are denoted by the dashed lines in panels a and b.

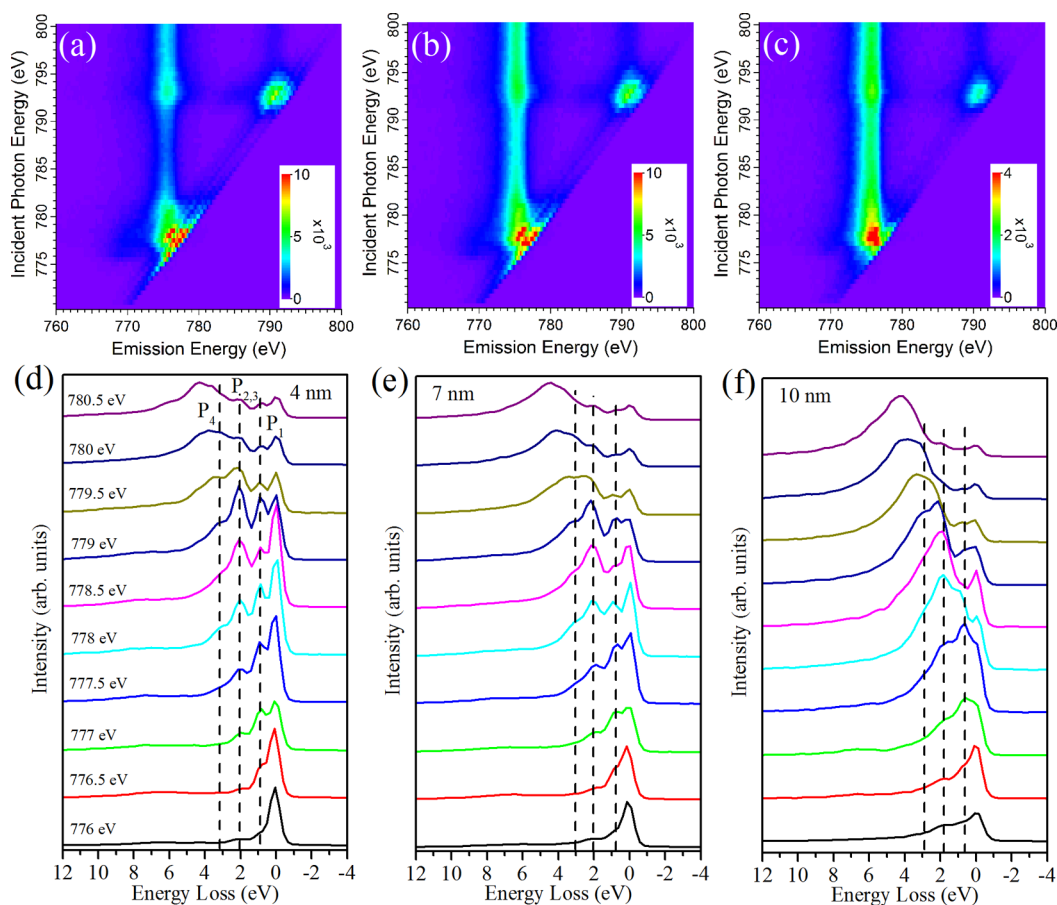


Figure 3. Co L-edge RIXS maps of (a) 4, (b) 7, and (c) 10 nm Co nanoparticles. The incident photon energy step used in producing these maps is 0.5 eV. Selected L-edge RIXS spectra of (d) 4, (e) 7, and (f) 10 nm Co nanoparticles around the Co L_3 threshold. The spectra are extracted from the RIXS maps in panels a–c. The incident photon energies are listed in panel d. The vertical dashed lines denote the features P_1 , $P_{2,3}$, and P_4 .

groups of manifolds located around 778 and 793 eV are related to the spin–orbit splitted Co 2p core levels (Co L_3 and L_2 edges, respectively).^{17,18} All three samples show a main peak at 777.5 eV (L_3 edge) and two weak shoulders at 776 and 778.5 eV. Compared with the reference spectra, these shoulders can be assigned to the contribution from oxide phase such as CoO. The presence of the shoulders in XAS spectra, stronger in 4 and 7 nm particles and weaker in 10 nm particles, suggests that all nanoparticles used in the current study are partially oxidized. Similar results were also reported in ambient-pressure X-ray photoelectron spectroscopy (APXPS) studies of Rh and Ru nanoparticles.^{19,20}

It is noticed that there are two strong satellite peaks at ~ 6 eV above the main Co L_3/L_2 absorption edges only in the TFY mode of XAS from 10 nm nanoparticles. Similar satellite peaks were previously reported and attributed to the metal-to-ligands charge transfer (MLCT) from the hybridization between transition metal $4p^*/3d$ and ligand π^* orbitals.^{16,21–23} In this regard, the satellite peaks seen in Figure 1e may come from the charge transfer between Co metal and ligands, whose details require further studies. When the surfaces of smaller nanoparticles are oxidized to a much higher degree, this MLCT effect is significantly suppressed beyond detection.

Figure 2 shows the M-edge XAS and RIXS spectra of 4, 7, and 10 nm Co nanoparticles. In the XAS spectra, the prominent peak around 61 eV corresponds to the Co M_3 absorption peak. Its energy position, as well as the pre-edge

feature around 59.5 eV that resembles the one in the XAS of CoO,²⁴ suggests that the surfaces of Co nanoparticles are oxidized. This aspect can be further examined by looking at the RIXS spectra shown in Figure 2a–c. Because the 3p core holes have extended wave functions that hybridize more strongly with the active occupied 3d orbitals, the transition metal M-edge RIXS spectra are often dominated by the strong elastic peak (zero energy loss) with extended tail, on top of which the RIXS features reside.

Three features denoted P_1 , P_2 , and P_3 (indicated by the dashed lines) can be seen in the RIXS spectra of 4 (Figure 2a) and 7 nm (Figure 2b) nanoparticles. Their intensities show strong resonance behavior when the incident photon energy (black ticks in the inset of Figure 2a) is tuned across Co M_3 edge. These peaks have been previously reported and assigned to the excitations between Co 3d states (d–d excitations).^{25–27} In the RIXS spectra of 4 nm Co nanoparticles, the peak P_1 has an energy loss of 0.93 eV and maximum intensity around 61 eV, consistent with the results from CoO.^{24,27} Thus we can attribute these d–d excitations to the presence of insulating oxide phase like CoO. With increasing particle size from 4 to 7 nm, P_1 becomes weaker and eventually disappears as in the case of 10 nm nanoparticles (Figure 2c). Because the delocalized 3p core holes can easily decay into the conduction bands in the metallic samples, leading to the suppression of RIXS signal, the intensity evolution of these d–d excitations implies that the metallicity increases with particle size. The disappearance of d–

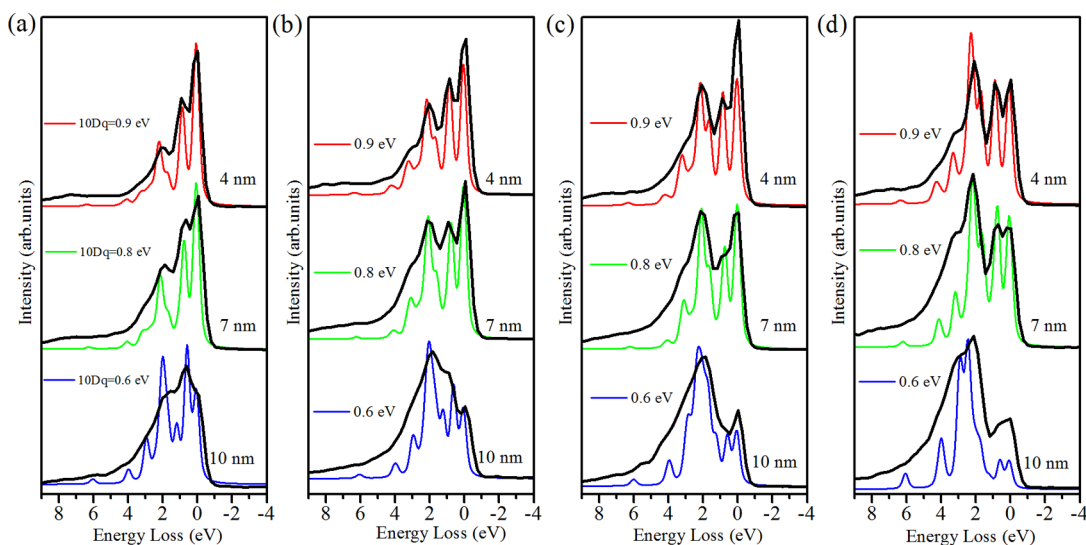


Figure 4. Comparison of simulated (thin colored curves) and experimental (thick black curves) Co L-edge RIXS spectra of 4 (top), 7 (middle), and 10 nm (bottom) Co nanoparticles at (a) 777.5, (b) 778, (c) 778.5, and (d) 779 eV incident photon energy. The intensities of these spectra are rescaled for clarity.

d excitations in the 10 nm nanoparticles can then be interpreted as due to the lower surface Co oxide to bulk Co metal volume ratio, leading to the extremely small M-edge RIXS cross-section beyond the detection limit; or in other words, the surface Co atoms in larger nanoparticles are more resistant to oxidation. Besides this intensity behavior, we also notice that the energy position of P_1 is changing with particle size: in 7 nm nanoparticles, it is reduced by roughly 0.1 eV. This point will be further discussed.

Although the M-edge RIXS spectroscopy offers much better energy resolution for resolving the d–d excitations, the extremely low RIXS cross-section prohibits us from studying the fine spectral structures. Therefore, we carried out the Co L-edge RIXS measurements. Figure 3a–c shows the L-edge RIXS maps (RIXS intensity displayed as a function of incident and emission photon energies) of 4, 7, and 10 nm Co nanoparticles. There are three main features in these RIXS maps: the strong diagonal line toward the bottom right part of the maps, the corresponding “parallel” diagonal lines, and vertical stripes around 776 and 792 eV emission energies. The strong diagonal line is the elastic line where the emission photon energy is the same as the incident photon energy (zero energy loss). The weaker diagonal lines parallel to the elastic line are the excitations with fixed energy loss. In this case, they are the Co 3d d–d and charge-transfer excitations. The vertical stripes are features with constant emission energies, and they are known to be the $L_{2,3}$ normal emissions from valence band transitions. In all RIXS maps, strong resonance effects are observed at both Co L_3 and L_2 thresholds, suggesting that the aforementioned features are intrinsic to the Co nanoparticles under study and not the experimental artifacts. We notice that the relative intensity of L_3 normal emissions (vertical stripe at 776 eV) to L_2/L_3 RIXS features increases dramatically with increasing particle size. Because the RIXS channel in bulk Co metal is suppressed by the competing Auger channel due to the enhanced decay of core holes in the intermediate state of metallic samples, which can also lead to much stronger L_3 normal emissions, this intensity ratio offers the direct measure of surface oxide phase relative to the interior Co metal phase. As particle size increases, the evolution of this intensity ratio

signifies the lower percentage of surface Co oxide and suggests that larger Co nanoparticles are more resistant to oxidation.

More information can be obtained by looking at the horizontal line cuts (fixed incident photon energies) in these RIXS maps. Figure 3d–f shows the selected L-edge RIXS spectra around the Co L_3 threshold. A broad set of weak peaks around 7 eV energy loss can be attributed to the charge-transfer excitations between Co 3d and O 2p orbitals.^{17,22} The pronounced d–d excitation peaks P_1 , $P_{2,3}$, and P_4 (indicated by the dashed lines) can be clearly seen in all spectra. The intensity of these d–d excitations exhibits a significant size-dependent behavior, implying noticeable changes in the 3d electronic states of surface Co atoms in these nanoparticles. In addition to the intensity behavior, we also notice that the energies of d–d excitations decrease slightly when the particle size increases, consistent with the M-edge RIXS results shown in Figure 2.

In the case of Co^{2+} under O_h crystal field, the spherical symmetric 4F ground state splits into ${}^4T_{1g}({}^4F)$, ${}^4T_{2g}({}^4F)$, and ${}^4A_{2g}({}^4F)$ multiplet states (see Figure 1a). The first peak P_1 in Figure 3d–f can be assigned to the transition from ${}^4T_{1g}({}^4F)$, the ground state in O_h symmetry, to ${}^4T_{2g}({}^4F)$ multiplet state.^{17,28} The second peak $P_{2,3}$ around 2 eV energy loss is the overlap of the transitions from ${}^4T_{1g}({}^4F)$ to ${}^4A_{2g}({}^4F)$ and ${}^4T_{1g}({}^4P)$.²⁸ The crystal-field splitting energy $10Dq$ value, which is the measure of the ligand field strength, can be estimated from the energy difference between ${}^4T_{1g}({}^4F)$ and ${}^4T_{2g}({}^4F)$ or between ${}^4T_{2g}({}^4F)$ and ${}^4A_{2g}({}^4F)$.^{28,29} Thus the $10Dq$ values of 4, 7, and 10 nm Co nanoparticles determined from the energy position of P_1 are ~ 0.9 , 0.8, and 0.6 eV, respectively.

To better understand the size-dependent intensity and energy of d–d excitations as well as the overall line shape of Co L-edge RIXS spectra, we performed the crystal-field multiplet simulations for Co^{2+} using the code developed by de Groot et al.^{30,31} The calculations simulate the $2p^63d^7 \rightarrow 2p^53d^8 \rightarrow 2p^63d^8\bar{d}$ transitions, where \bar{d} denotes a hole in the Co^{2+} 3d levels. Figure 4 shows the comparison of experimental (thick black curves) and simulated (thin colored curves) RIXS spectra. Although the experimental RIXS spectra do not exhibit rich structures as the simulated ones, presumably due to much

worse experimental energy resolution, the agreement between them is satisfactory considering that there are no other free parameters to tweak in these multiplet calculations and the agreement extends over several incident photon energies. This implies that the multiplet parameters are correctly chosen and the simulations capture the essence of RIXS spectra. Although the normal emissions from Co metal may complicate the RIXS simulations, we can see that the simulations still agree very nicely with the experimental RIXS spectra for excitation energies at 775.5, 778, and 778.5 eV, in particular for the energies and relative intensities of d–d excitations. The discrepancy becomes noticeable for the excitation energy at 779 eV, which indicates that the normal emission may become a contribution that cannot be ignored in the comparison. We would like to emphasize that the normal emission contribution is very low at the resonant excitations, as seen in the RIXS maps in Figure 3a–c, and thus the RIXS profiles around the resonance should still be dominated by d–d excitations.

To investigate the influence of annealing and reduction process on the electronic structures, the as-prepared 4 and 7 nm Co nanoparticles were further annealed in air to remove the ligands and then reduced by H₂. Figure 5 shows the TEM and

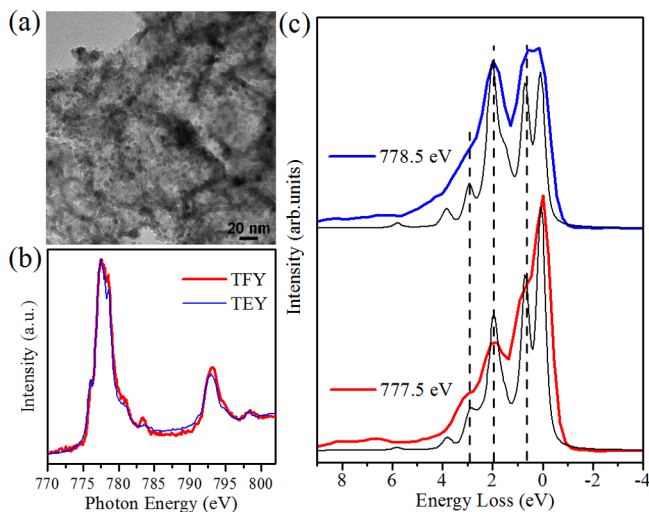


Figure 5. (a) TEM image (scale bar: 20 nm), (b) XAS, and (c) RIXS spectra of 4 nm Co nanoparticles after both annealing and reduction treatments. In panel c, the thick colored and thin black curves are the experimental and simulated spectra, respectively.

L-edge XAS/RIXS results of 4 nm nanoparticles after both annealing and reduction treatments. The results of 4 nm nanoparticles after annealing only and 7 nm nanoparticles after both annealing and reduction can be found in the Supporting Information. The TEM image in Figure 5a shows that after these treatments most nanoparticles of 4 nm samples retain their original size, except some are sintered together. The sintering leads to an increase in average size by roughly 1 nm. The XAS spectra of treated 4 nm nanoparticles (Figure 5b) indicate that the nanoparticles mainly consist of Co metal and their surface is still slightly oxidized. Interestingly, we can see that the MLCT peaks similar to the ones seen in the 10 nm as-prepared nanoparticles start to show up. This suggests that the treated 4 nm nanoparticles behave more similar to larger untreated nanoparticles. As the oleic acid was already removed, the MLCT peaks probably come from the charge transfer between Co metal and some other species, but the nature of

this MLCT effect requires further studies. The RIXS spectra (thick colored curves) of treated 4 nm nanoparticles at selected incident photon energies are shown in Figure 5c, overlaid with multiplet simulations (thin black curves). It is found that to reach a better agreement between them the 10Dq value needs to be reduced from 0.9 to 0.7 eV. This reflects the fact that the electronic structures of nanoparticles were changed during the annealing and reduction process. One possibility is that the reduced 10Dq is the outcome of size increase, as seen in the TEM images, and this conjecture is in line with the RIXS results of the as-prepared Co nanoparticles.

The significant size-dependent d–d excitations and crystal-field splitting energy 10Dq of Co nanoparticles signify the strong modulation on the electronic structures by particle size. We think that varying 10Dq could be related to the oxidation of surface Co atoms. The structure of surface Co oxide phase could be very different when Co nanoparticles are oxidized to different levels. For instance, if the surface Co oxide is in lower symmetry than O_h symmetry, the reduced 10Dq could be observed.²⁹ The reduced 10Dq in larger Co nanoparticles indicates weaker interactions between Co and O atoms, or equivalently, the weaker Co–O bond. This weaker Co–O bond is in agreement with the finding that larger Co nanoparticles are more resilient to oxidation. It is reported that the Co–O bond forms during the CO dissociation on the surface of Co nanoparticles in the FT reaction.^{4,32} Thus the variation of Co–O bond strength with respect to particle size can play a critical role in the size-dependent catalytic performance of Co nanoparticles.

In summary, the electronic structures of 4, 7, and 10 nm Co nanoparticles are studied using XAS and RIXS spectroscopies at Co M- and L-edges. Both XAS and RIXS results suggest the decrease in Co–O bond strength with increased Co nanoparticle size. Furthermore, our RIXS results clearly reveal the significant size-dependent d–d excitations. The crystal-field splitting energy 10Dq in the 4, 7, and 10 nm Co nanoparticles are determined to be ~0.9, 0.8, and 0.6 eV, respectively. The evolution of the intensity of d–d excitations and the reduction of 10Dq in larger Co nanoparticles are confirmed from the multiplet simulations of Co²⁺. These findings signify the modulation of electronic structures of Co nanoparticles as a function of particle size, which bring in new insight into the size-dependent catalytic performance of Co nanoparticles.

METHODS

Sample Preparation. Monodispersed Co nanoparticles with sizes of 4, 7, and 10 nm were synthesized by decomposing the carbonyl precursor Co₂(CO)₈ in *o*-dichlorobenzene in the presence of oleic acid at 180, 172, and 168 °C, respectively.³³ The size of nanoparticles was precisely controlled by the heating temperature and determined by the transmission electron microscopy (TEM). In a typical synthesis, oleic acid (130 mg) was evacuated for 30 min, and anhydrous *o*-dichlorobenzene (15 mL) was then added under Ar environment. While vigorously stirring, the solution was heated to certain temperature and was kept at that temperature for 30 min. Then Co₂(CO)₈ (512 mg) in *o*-dichlorobenzene (3 mL) was injected quickly into this solution. This colloidal solution was kept at the same temperature for another 20 min prior to stopping the heating and cooling the flask in a flow of Ar gas. The particles were precipitated by 2-propanol and collected by centrifugation and then were redispersed in hexane. The nanoparticles were then washed twice with hexane and 2-

propanol and stored in hexane for further studies. The liquid-suspended nanoparticles were dropped onto silicon wafers in the glovebox under a nitrogen atmosphere. The as-prepared 4 and 7 nm Co nanoparticles were loaded onto silica support (MCF-17), annealed at 350 °C in air for 1 h to remove the capping ligands, and then reduced at 350 °C in H₂/Ar (10% H₂) for 2 h. The powder of silica support was pressed into nickel foil in the glovebox. All samples were mounted onto experimental holders and placed inside a portable vacuum suitcase in the glovebox. Then, the samples were directly transferred from the vacuum suitcase into the experimental chamber without exposing to air to avoid reoxidation or contamination.

XAS and RIXS Measurements. The M- and L-edge XAS/RIXS measurements were performed at beamlines 4.0.3 and 8.0.1 at the Advanced Light Source (ALS), Lawrence Berkeley National Laboratory (LBNL), respectively. All measurements were performed at room temperature and under vacuum pressure of $\sim 1 \times 10^{-8}$ Torr for L-edge measurements ($\sim 4 \times 10^{-10}$ Torr for M-edge measurements). The XAS spectra were recorded in both TEY (sample-to-ground drain current) and TFY modes and normalized by the incident photon flux determined from the photocurrent of an upstream Au mesh. For RIXS measurements, the incident photon polarization was linear in the horizontal scattering plane (π -polarization). The scattered photons from samples were recorded by X-ray spectrometers at 90° angle relative to the incident photon beam. The combined energy resolution for M-edge and L-edge RIXS determined from the full width at half-maximum (fwhm) of elastic peak is about 0.025 and 0.5 eV, respectively.

Multiplet Calculation. The Co L-edge RIXS spectra are simulated using the code developed by de Groot et al. For simplicity, we do not include the charge-transfer effect. The Coulomb repulsion, exchange interaction, and 3d spin-orbit interaction are reduced to 64, 64, and 80% of the Hartree-Fock values, respectively. The linear-horizontal polarization scattering geometry is simulated by using the equal sum of [σ_{in} to π_{out}] and [π_{in} to σ_{out}] polarizations.²⁹ The octahedral symmetry is used, and the crystal-field splitting parameter 10Dq is set to the experimental values: 0.9, 0.8, and 0.6 eV for 4, 7, and 10 nm nanoparticles.

■ ASSOCIATED CONTENT

● Supporting Information

The Supporting Information is available free of charge on the ACS Publications website at DOI: [10.1021/acs.jpclett.6b02600](https://doi.org/10.1021/acs.jpclett.6b02600).

Source and purity of related chemicals and the synthesis of MCF-17; size distribution; energies of crystal-field multiplet simulation parameters used in RIXS simulations; TEM images, and L-edge XAS/RIXS of 4 and 7 nm Co nanoparticles after annealing and reduction treatments. (PDF)

■ AUTHOR INFORMATION

Corresponding Authors

*Y.C.: E-mail: ychuang@lbl.gov.

*J.G.: E-mail: jguo@lbl.gov.

ORCID

Jinghua Guo: [0000-0002-8576-2172](https://orcid.org/0000-0002-8576-2172)

Author Contributions

The manuscript was written through contributions of all authors. All authors have given approval to the final version of the manuscript.

Notes

The authors declare no competing financial interest.

■ ACKNOWLEDGMENTS

The Advanced Light Source is supported by the Director, Office of Science, Office of Basic Energy Sciences of the U.S. Department of Energy under contract no. DE-AC02-05CH11231. This work is supported by the Office of Basic Energy Sciences (BES), Division of Materials Sciences and Engineering, of the U.S. Department of Energy (DOE) under contract no. DE-AC02-05CH11231, through the Chemical and Mechanical Properties of Surfaces, Interfaces and Nanostructures program (FWP KC3101). Z.Z.C. acknowledges fellowship support from the University of Science and Technology of China. C.X. acknowledges support from Suzhou Industrial Park fellowship. X.L. and X.F. acknowledge the support of the National Natural Science Foundation of China (21473235, 11227902), One Hundred Person Project of the Chinese Academy of Sciences.

■ REFERENCES

- (1) Khodakov, A. Y.; Chu, W.; Fongarland, P. Advances in the Development of Novel Cobalt Fischer-Tropsch Catalysts for Synthesis of Long-Chain Hydrocarbons and Clean Fuels. *Chem. Rev.* **2007**, *107*, 1692–1744.
- (2) Iglesia, E. Design, Synthesis, and Use of Cobalt-Based Fischer-Tropsch Synthesis Catalysts. *Appl. Catal., A* **1997**, *161*, 59–78.
- (3) Bezemer, G. L.; Bitter, J. H.; Kuipers, H.; Oosterbeek, H.; Holewijn, J. E.; Xu, X. D.; Kapteijn, F.; van Dillen, A. J.; de Jong, K. P. Cobalt Particle Size Effects in the Fischer-Tropsch Reaction Studied with Carbon Nanofiber Supported Catalysts. *J. Am. Chem. Soc.* **2006**, *128*, 3956–3964.
- (4) Tuxen, A.; Carenco, S.; Chintapalli, M.; Chuang, C. H.; Escudero, C.; Pach, E.; Jiang, P.; Borondics, F.; Beberwyck, B.; Alivisatos, A. P.; Thornton, G.; Pong, W. F.; Guo, J. H.; Perez, R.; Besenbacher, F.; Salmeron, M. Size-Dependent Dissociation of Carbon Monoxide on Cobalt Nanoparticles. *J. Am. Chem. Soc.* **2013**, *135*, 2273–2278.
- (5) Jacobs, G.; Das, T. K.; Zhang, Y. Q.; Li, J. L.; Racoillet, G.; Davis, B. H. Fischer-Tropsch Synthesis: Support, Loading, and Promoter Effects on the Reducibility of Cobalt Catalysts. *Appl. Catal., A* **2002**, *233*, 263–281.
- (6) Schanke, D.; Hilmen, A. M.; Bergene, E.; Kinnari, K.; Rytter, E.; Adnanes, E.; Holmen, A. Reoxidation and Deactivation of Supported Cobalt Fischer-Tropsch Catalysts. *Energy Fuels* **1996**, *10*, 867–872.
- (7) den Breejen, J. P.; Radstake, P. B.; Bezemer, G. L.; Bitter, J. H.; Froseth, V.; Holmen, A.; de Jong, K. P. On the Origin of the Cobalt Particle Size Effects in Fischer-Tropsch Catalysis. *J. Am. Chem. Soc.* **2009**, *131*, 7197–7203.
- (8) Yang, J.; Tveten, E. Z.; Chen, D.; Holmen, A. Understanding the Effect of Cobalt Particle Size on Fischer-Tropsch Synthesis: Surface Species and Mechanistic Studies by Ssitka and Kinetic Isotope Effect. *Langmuir* **2010**, *26*, 16558–16567.
- (9) Herranz, T.; Deng, X.; Cabot, A.; Guo, J.; Salmeron, M. Influence of the Cobalt Particle Size in the Co Hydrogenation Reaction Studied by in Situ X-Ray Absorption Spectroscopy. *J. Phys. Chem. B* **2009**, *113*, 10721–10727.
- (10) Geerlings, J. J. C.; Zonneville, M. C.; Degroot, C. P. M. Structure Sensitivity of the Fischer-Tropsch Reaction on Cobalt Single-Crystals. *Surf. Sci.* **1991**, *241*, 315–324.
- (11) Prieto, G.; Martinez, A.; Concepcion, P.; Moreno-Tost, R. Cobalt Particle Size Effects in Fischer-Tropsch Synthesis: Structural

and in Situ Spectroscopic Characterisation on Reverse Micelle-Synthesised Co/ITQ-2 Model Catalysts. *J. Catal.* **2009**, *266*, 129–144.

(12) Kotani, A.; Shin, S. Resonant Inelastic X-Ray Scattering Spectra for Electrons in Solids. *Rev. Mod. Phys.* **2001**, *73*, 203–246.

(13) Hatton, P. D.; Wilkins, S. B.; Beale, T. A. W.; Johal, T. K.; Prabhakaran, D.; Boothroyd, A. T. Resonant Soft X-Ray Scattering—a New Probe of Charge, Spin and Orbital Ordering in the Manganites. *J. Magn. Mater.* **2005**, *290–291*, 891–897.

(14) Ament, L. J. P.; van Veenendaal, M.; Devereaux, T. P.; Hill, J. P.; van den Brink, J. Resonant Inelastic X-Ray Scattering Studies of Elementary Excitations. *Rev. Mod. Phys.* **2011**, *83*, 705–767.

(15) Luo, Y.; Agren, H.; Gelmukhanov, F.; Guo, J. H.; Skytt, P.; Wassdahl, N.; Nordgren, J. Symmetry-Selective Resonant Inelastic X-Ray-Scattering of C-60. *Phys. Rev. B: Condens. Matter Mater. Phys.* **1995**, *52*, 14479–14496.

(16) Liu, H. J.; Guo, J. H.; Yin, Y. D.; Augustsson, A.; Dong, C. L.; Nordgren, J.; Chang, C. L.; Alivisatos, P.; Thornton, G.; Ogletree, D. F.; Requejo, F. G.; de Groot, F.; Salmeron, M. Electronic Structure of Cobalt Nanocrystals Suspended in Liquid. *Nano Lett.* **2007**, *7*, 1919–1922.

(17) Magnuson, M.; Butorin, S. M.; Guo, J. H.; Nordgren, J. Electronic Structure Investigation of CoO by Means of Soft X-Ray Scattering. *Phys. Rev. B: Condens. Matter Mater. Phys.* **2002**, *65*, 205106.

(18) Cui, Z.; Xu, H.; Yun, Y.; Guo, J.; Chuang, Y.-D.; Huang, H.; Meng, D.; Wang, J.; Fu, Z.; Peng, R.; Knize, R. J.; Brown, G. J.; Zhai, X.; Lu, Y. Soft X-Ray Absorption Spectroscopy Investigations of Bi₄FeCoTi₃O₁₈ and LaBi₃FeCoTi₃O₁₈ Epitaxial Thin Films. *J. Appl. Phys.* **2016**, *120*, 084101.

(19) Grass, M. E.; Zhang, Y.; Butcher, D. R.; Park, J. Y.; Li, Y.; Bluhm, H.; Bratlie, K. M.; Zhang, T.; Somorjai, G. A. A Reactive Oxide Overlayer on Rhodium Nanoparticles During Co Oxidation and Its Size Dependence Studied by in Situ Ambient-Pressure X-Ray Photoelectron Spectroscopy. *Angew. Chem., Int. Ed.* **2008**, *47*, 8893–8896.

(20) Qadir, K.; Joo, S. H.; Mun, B. S.; Butcher, D. R.; Renzas, J. R.; Aksoy, F.; Liu, Z.; Somorjai, G. A.; Park, J. Y. Intrinsic Relation between Catalytic Activity of Co Oxidation on Ru Nanoparticles and Ru Oxides Uncovered with Ambient Pressure XPS. *Nano Lett.* **2012**, *12*, 5761–5768.

(21) Hatsui, T.; Takata, Y.; Kosugi, N. Strong Metal-to-Ligand Charge Transfer Bands in Ni 2p Photoabsorption of K₂Ni(CN)₄·H₂O. *Chem. Phys. Lett.* **1998**, *284*, 320–324.

(22) Hatsui, T.; Takata, Y.; Kosugi, N. Strong Metal-to-Ligand Charge Transfer Bands Observed in Ni K- and L-Edge XANES of Planar Ni Complexes. *J. Synchrotron Radiat.* **1999**, *6*, 376–378.

(23) Moulin, C. C. D.; Villain, F.; Bleuzen, A.; Arrio, M. A.; Sainctavit, P.; Lomenech, C.; Escax, V.; Baudalet, F.; Dartyge, E.; Gallet, J. J.; Verdager, M. Photoinduced Ferrimagnetic Systems in Prussian Blue Analogues C^xCo₄[Fe(CN)₆]_y (C¹ = Alkali Cation). 2. X-Ray Absorption Spectroscopy of the Metastable State. *J. Am. Chem. Soc.* **2000**, *122*, 6653–6658.

(24) Wray, L. A.; Li, J.; Qiu, Z. Q.; Wen, J.; Xu, Z.; Gu, G.; Huang, S.-W.; Arenholz, E.; Yang, W.; Hussain, Z.; Chuang, Y.-D. Measurement of the Spectral Line Shapes for Orbital Excitations in the Mott Insulator CoO Using High-Resolution Resonant Inelastic X-Ray Scattering. *Phys. Rev. B: Condens. Matter Mater. Phys.* **2013**, *88*, 035105.

(25) Augustsson, A.; Henningsson, A.; Butorin, S. M.; Siegbahn, H.; Nordgren, J.; Guo, J. H. Lithium Ion Insertion in Nanoporous Anatase TiO₂ Studied with Rixs. *J. Chem. Phys.* **2003**, *119*, 3983–3987.

(26) Schmitt, T.; Duda, L. C.; Matsubara, M.; Augustsson, A.; Trif, F.; Guo, J. H.; Gridneva, L.; Uozumi, T.; Kotani, A.; Nordgren, J. Resonant Soft X-Ray Emission Spectroscopy of Doped and Undoped Vanadium Oxides. *J. Alloys Compd.* **2004**, *362*, 143–150.

(27) Chiuzbăian, S. G.; Schmitt, T.; Matsubara, M.; Kotani, A.; Ghiringhelli, G.; Dallera, C.; Tagliaferri, A.; Braicovich, L.; Scagnoli, V.; Brookes, N. B.; Staub, U.; Patthey, L. Combining M- and L-Edge Resonant Inelastic X-Ray Scattering for Studies of 3d Transition Metal Compounds. *Phys. Rev. B: Condens. Matter Mater. Phys.* **2008**, *78*, 245102.

(28) van Schooneveld, M. M.; Kurian, R.; Juhin, A.; Zhou, K.; Schlappa, J.; Strocov, V. N.; Schmitt, T.; de Groot, F. M. F. Electronic Structure of CoO Nanocrystals and a Single Crystal Probed by Resonant X-Ray Emission Spectroscopy. *J. Phys. Chem. C* **2012**, *116*, 15218–15230.

(29) Liu, B.; Wang, R. P.; Glass, E. N.; Hill, C. L.; Cuk, T.; Okamoto, J.; Huang, D. J.; van Schooneveld, M. M.; de Groot, F. M. Distorted Tetrahedral Co^{II} in K₃H[CoW₁₂O₄₀]·xH₂O Probed by 2p3d Resonant Inelastic X-Ray Scattering. *Inorg. Chem.* **2016**, *55*, 10152–10160.

(30) de Groot, F. Multiplet Effects in X-Ray Spectroscopy. *Coord. Chem. Rev.* **2005**, *249*, 31–63.

(31) Bazin, D.; Kovács, I.; Guzzi, L.; Parent, P.; Laffon, C.; De Groot, F.; Ducreux, O.; Lynch, J. Genesis of Co/SiO₂ Catalysts: XAS Study at the Cobalt L_{III,II} Absorption Edges. *J. Catal.* **2000**, *189*, 456–462.

(32) Shetty, S.; van Santen, R. A. Co Dissociation on Ru and Co Surfaces: The Initial Step in the Fischer–Tropsch Synthesis. *Catal. Today* **2011**, *171*, 168–173.

(33) Iablokov, V.; Beaumont, S. K.; Alayoglu, S.; Pushkarev, V. V.; Specht, C.; Gao, J.; Alivisatos, A. P.; Kruse, N.; Somorjai, G. A. Size-Controlled Model Co Nanoparticle Catalysts for CO₂ Hydrogenation: Synthesis, Characterization, and Catalytic Reactions. *Nano Lett.* **2012**, *12*, 3091–3096.